An Automated Analysis Program for the Evaluation of Cardiac PET Studies: Initial Results in the Detection and Localization of Coronary Artery Disease Using Nitrogen-13-Ammonia

Christian Laubenbacher*, Jill Rothley, Joe Sitomer, Rob Beanlands, Stephen Sawada, Ron Sutor, David Muller and Markus Schwaiger

Divisions of Nuclear Medicine and Cardiology, Department of Internal Medicine, University of Michigan, Ann Arbor, Michigan

Positron emission tomography (PET), in combination with myocardial blood flow tracers, allows highly accurate diagnosis of coronary artery disease using visual data interpretation. To increase the objectivity of data analysis and to reduce interobserver variability, we developed an automated analysis method for the three-dimensional definition of myocardial activity, which includes true volumetric data extraction and mathematical constraints of activity sampling to the expected shape of the left ventricle. Data are displayed in a standardized polar map or three-dimensional format for comparison with a normal database. The first clinical evaluation of this method in 52 patients using receiver operating characteristics (ROC) curve analysis demonstrated high diagnostic accuracy for detection as well as localization of coronary artery stenosis in predefined vascular territories. The interobserver and intraobserver agreement for localization of disease was excellent, with correlation coefficients varying from 0.85 to 0.99 for individual vascular territories. Thus, this automated quantitative analysis program provides highly accurate and reproducible evaluation of cardiac PET flow studies. Definite determination of its diagnostic accuracy requires a prospective multicenter trial in a larger patient population employing the criteria for abnormality established in this initial clinical evaluation.

J Nucl Med 1993; 34:968–978

Positron emission tomography (PET) is an advanced scintigraphic imaging technique which permits the accurate assessment of regional tissue tracer distribution. In combination with blood flow tracers such as ^{82}Rb and ^{13}N-ammonia, this technique has been shown to provide highly accurate detection of coronary artery disease (CAD) (*1–4*). Studies comparing ^{82}Rb PET imaging with ^{201}Tl single-photon emission computed tomography (SPECT) imaging in the same patient population have demonstrated the diagnostic superiority of PET. This diagnostic advantage is thought to reflect the use of attenuation correction and, thus, avoidance of attenuation artifacts, which frequently cause false-positive ^{201}Tl SPECT findings (*5,6*).

Most of these previous PET studies employed visual analysis of myocardial tracer distribution under rest and stress conditions. Semiquantitative analysis using circumferential profile techniques has been successfully employed in combination with SPECT cardiac imaging to yield objective definition of regional scintigraphic abnormalities (*5–7*). Only a few methods, however, have been introduced for similar analysis of cardiac PET flow studies (*8,9*). The need for the development of quantitative analysis methods for PET for the more objective assessment of regional perfusion abnormalities and the reduction of interobserver and intraobserver variability is well recognized. Since PET-derived measurements of tissue tracer concentrations are truly quantitative, the application of such techniques may allow accurate definition of tracer uptake abnormalities and provide a sensitive means to define the extent and severity of regional perfusion defects to yield improved quantification of the severity of CAD.

The purpose of this study was to introduce a quantitative analysis approach which employs truly volumetric data sampling and mathematically constrained searching routines for automated definition of myocardial activity. This method has been employed in a control group of subjects without evidence of CAD and in patients with angiographically proven CAD in order to define its diagnostic performance in a test population and to develop diagnostic criteria for regional abnormalities which can subsequently be

Received Aug. 24, 1992; revision accepted Jan. 14, 1993.

For correspondence or reprints contact: Markus Schwaiger, MD, Division of Nuclear Medicine, University of Michigan Medical Center, B1G505 1500 E. Medical Center Dr., Ann Arbor, MI 48109-0028.

*Current address: Nuklearmedizinische Klinik und Poliklinik der Technischen Universitat Muenchen Klinikum rechts der Isar, Muenchen, Germany.

used for prospective testing of this method in a clinical trial to determine its diagnostic accuracy.

METHODS

Patient Population

The study population consisted of 52 subjects who had undergone ^{13}N-ammonia PET studies in combination with pharmacologic stress studies. Twenty-three subjects had low likelihood of CAD (<5% likelihood of disease), whereas 29 patients underwent coronary angiography within 3 mo of the PET study. No patient had a history of unstable angina intervention or myocardial infarction within 6 mo of the time of the study; nor had any patients undergone percutaneous coronary angioplasty (PTCA) or coronary artery bypass graft (CABG) between angiography and the PET study. Informed consent was obtained from all persons participating in this study. The imaging protocol was approved by the Institutional Review Board of the University of Michigan Medical Center.

PET

All patients were studied after an overnight fast. Patients were prohibited from consuming caffeinated beverages in the 24 hr prior to testing. Theophylline-containing medications were withheld for at least 48 hr prior to PET imaging. None of the patients had pulmonary symptoms prior to pharmacologic stress testing. Patients were positioned in a 15-slice whole-body PET Scanner (931 CTI/Siemens, Knoxville, TN), which has eight circular detector rings to allow for the simultaneous acquisition of 15 contiguous transaxial images with a slice thickness of 6.75 mm. The reconstructed in-plane image resolution of this system is 6 mm FWHM and the axial resolution is 8 mm FWHM using line source phantoms.

In order to verify the correct position of the detectors over the heart, a 2-min scout scan was performed postinjection of 74 MBq ^{13}N-ammonia (acquisition time: 4 min). Afterwards, a transmission scan using a retractable ^{68}Ge ring source was performed for 15 to 20 min (100 to 200 million counts). The transmission scan was followed by a baseline ^{13}N-ammonia study, which consisted of the infusion of 740 MBq ^{13}N-ammonia (specific activity: 74 MBq/ml). The agent was infused over 30 sec with a Harvard pump. Three minutes after the end of ^{13}N-ammonia infusion, data were acquired for 10 min.

Pharmacologic Stress Testing

Fifty minutes after the rest studies, intravenous infusion of either dipyridamole (Persantine, Boehringer-Ingelheim, Germany: 0.142 mg/kg · min for 4 min) or adenosine (Medco Research, Los Angeles, CA; 140 μg/kg · min for 6 min) was started. Five minutes after the end of the dipyridamole infusion, or 3 min after the beginning of the adenosine infusion, the injection of the second ^{13}N-ammonia dose (740 MBq) was started. The stress protocols are similar to those employed by other groups for dipyridamole (*10–12*) and adenosine (*13–15*).

Three minutes after administration of ^{13}N-ammonia, stress data acquisition was started (acquisition time: 10 min). Continuous heart rate, blood pressure and multilead ECG monitoring were performed every minute during vasodilator infusion and then recorded every 2 min to the end of the studies.

Analysis of PET Images

All PET data were reconstructed into images which represented myocardial ^{13}N activity from 3–10 min after tracer injection. The rest and stress images were analyzed by two observers

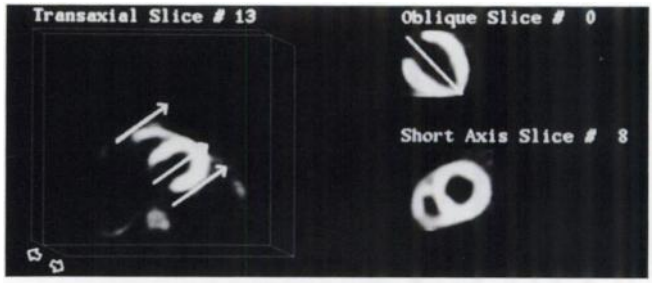

FIGURE 1. Operator-Interaction 1. Identification of center lines in transaxial (left upper corner) and oblique slices (right upper corner) with adjustment of the free walls of the right and left ventricle. The resulting conventional short-axis views are demonstrated in the lower panel.

blinded to the patient's history or coronary angiography results. Image analysis was performed using a Sun SPARC Station 2 (Sun Microsystems, Mountain View, CA) and involved three distinct steps:

1. Interactive three-dimensional definition of the long-axis of the left ventricle.
2. Automatic volumetric radial search for activity maxima.
3. Comparison of individual patient data with a reference database.

Furthermore, data processing included the definition of regional abnormalities in predefined vascular territories and data display using either a polar map format or three-dimensional projection of the data on an ellipsoid resembling the shape of the left ventricle.

Definition of Myocardial Activity. The 15 acquired transaxial tomographic slices were interpolated into an isotropic volume. A mid left ventricular transaxial plane was subsequently selected for the interactive definition of the long-axis as well as the lateral borders of the left and right ventricle (Fig. 1). In order to delineate the long-axis in three dimensions, a second image plane perpendicular to the initial transaxial plane was displayed and the long-axis again was interactively defined. These images were also used to mark the base and apex of the left ventricle as well as the posterior intersection of the right and left ventricle as depicted in Figure 2. This marking of the ventricular intersection defined the spatial standardization of myocardial activity display and was set by convention to 102° (*16*). The three-dimensionally defined long-axis represented the starting point for a radial search of myocardial activity. Starting at the most basal aspect of the long-axis and the posterior intercept of right and left ventricle, 36 radial activity profiles were automatically extracted perpendicular to the long-axis at ten equally spaced planes, covering the proximal 75% of the long-axis. In the distal 25% of the long-axis, spherical sampling was employed to follow the shape of the left ventricle and provide radial activity profiles perpendicular to the myocardium,

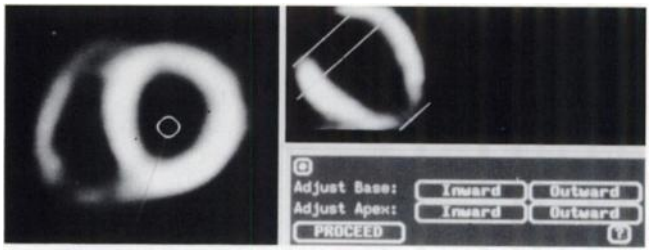

FIGURE 2. Definition of "search range" at base and apex of left ventricle and delineation of right/left ventricle intercept.

resulting in an overall "bottle brush" search pattern. The angular interval between profiles was increased in the apical zone in inverse proportion to the expected decrease in myocardial surface area to maintain consistent sampling density (Fig. 3).

The activity maxima search was subsequently performed on each radial profile in order to locate the center of myocardial activity. The radial activity profile of each radial search was smoothed and the average maximum values were calculated using criteria for flatness to minimize the effect of myocardial defects on the detection of the signal defined as:

$$\text{maximum/average activity} > k/F,$$

where k represents an empirically determined constant and F is a constant for flatness (Fig. 4):

$$F = \sqrt{\frac{\text{maximal activity}}{\text{area under profile}}}.$$

Based on these criteria, regional maximal activity was determined and assumed to reflect myocardial activity. If these criteria were not met, the myocardial location was determined by interpolating the distance from the long-axis to the maxima of neighboring points. This initial search resulted in a first estimate of the location of activity maxima. Myocardial activity was subsequently sampled using a 3 × 3 × 3 median filter centered around the defined maximal activity.

Following this first-pass search, a second constraining process for the definition of continuity of the detected myocardial activity was employed. This second-pass employs an algorithm for shape and continuity constraint, which minimizes sampling errors in regions with severe tracer uptake defects as well as segments with high extracardiac activity. For each plane perpendicular to the long-axis, the second derivative of the angular radius function was calculated. The second derivative was chosen due to its sensitivity to nondirectional breaks in continuity. The point corresponding to the maximum second derivative was marked as "suspect." The second derivative function was then recalculated omitting this point. This iterative process continued until the maximum second derivative value fell below an empirically determined value. The remaining accepted points were then used to constrain a repeated maxima search to the most likely location of the myocardium.

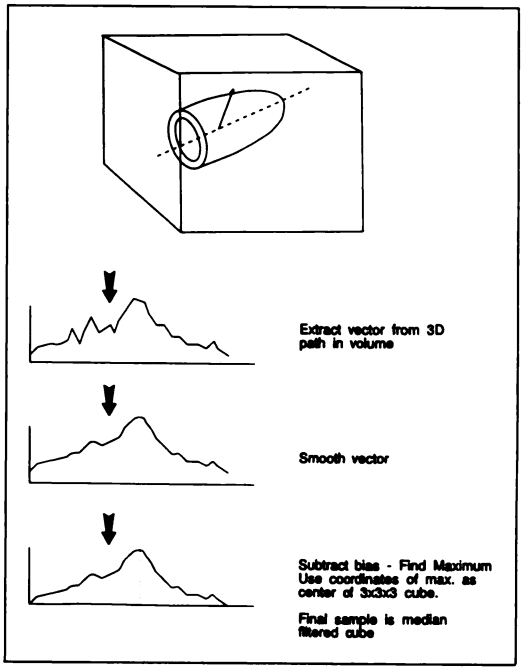

FIGURE 4. Three-dimensional vector processing. Each three-dimensional vector "bristle" in the bottlebrush sampling pattern is extracted along the operator defined long-axis. The resulting activity profiles (vector) are smoothed and the maximal activity defined as center of 3 × 3 × 3 voxels cube (see text for more details). The arrows correspond to the stepwise approach.

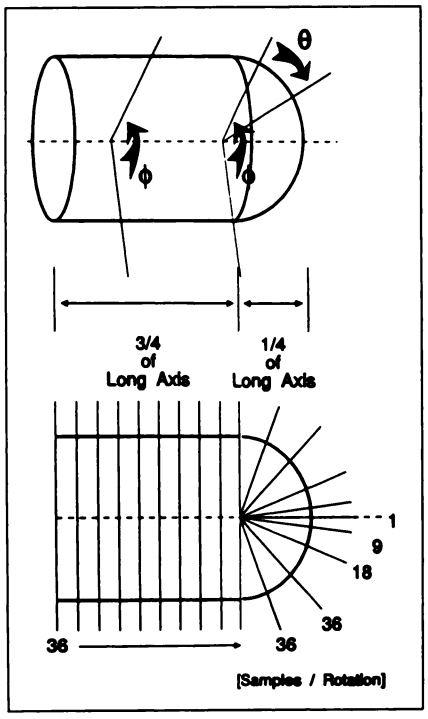

FIGURE 3. "Bottle brush" sampling pattern for definition of myocardial activity distribution. Over the basal 75% of the long-axis, a cylindrical sampling pattern at 10 equally spaced planes with 36 radial profiles perpendicular to the long-axis is used. In the apical 25% of the long-axis, a spherical sampling with increasing angular intervals in the apical zone is employed to maintain consistent sampling density due to the decrease in myocardial surface area.

Comparison with a Reference Database. Following this two-pass search process, regionally determined myocardial activity was normalized to the "maximal activity" within a given image volume. This "maximal activity" was determined by the average activity of a 50° wedge consisting of two contiguous rings moved across the surface of the heart excluding the two most basal and four most apical rings. The maximal value of this three-dimensional moving function was considered to represent "maximal activity" and was set to 100%. All previously defined radial activity maxima were then normalized to this value and expressed as a percentage. Data were stored in a three-dimensional matrix of regional relative tracer retention and compared to an average "normal" matrix defined by a reference group of individuals without cardiac disease. As commonly used for SPECT, the data were displayed in polar map format. Representative vascular territories for the major coronary arteries were adopted from previously published analysis approaches for SPECT (*16*).

Criteria for Abnormality. Regional tracer uptake abnormalities were expressed in terms of extent and severity using standard deviation criteria based on the normal distribution of tracer within the left ventricle. Extent of tracer uptake abnormalities was expressed as percent of pixels within a given vascular territory below the predefined standard deviation criteria. The severity of tracer defect was defined as average standard deviation in those pixels falling below the standard deviation criteria. For this study, the standard deviation criteria varied from 1 to 3, whereas a defect

extent of >10% was considered abnormal in each vascular territory. In addition, the rest and stress data were compared in order to develop criteria for stress-induced perfusion abnormalities. Two approaches were employed: the difference (rest-stress map) and the ratio (rest-to-stress map). Again, individual subtraction and ratio data were compared with corresponding normal values. Standard deviation criteria and extent criteria were used as outlined above.

The only interaction by the operator during this data analysis was the definition of the long-axis, the delineation of base and apex and the identification of the intercept of the left and right ventricle. The time required for the search, computing and display of results was less than 5 min, which allowed rapid analysis of each image volume.

Coronary Angiography

The interval between PET studies and cardiac catheterization was less than 3 mo. Quantitative coronary angiography was applied using a ADAC system (ADAC Laboratories, Milpitas, CA) and a single plane approach, which has been previously published (*17*). The following angiographic criteria were used to define the presence of significant artery stenosis:

1. Quantitatively determined diameter stenosis ≥50%.
2. Quantitatively determined diameter stenosis ≥75%.
3. Quantitatively determined diameter stenosis ≥90%.

Stenoses were categorized as involving the left anterior descending (LAD), left circumflex (LCx) or right coronary artery (RCA). For comparison with the PET studies, left main coronary lesions were included as both LAD and LCx disease. Diagonal branches were grouped with the LAD, marginal branches with the LCx and lesions of the posterolateral and posterior descending arteries with the RCA.

Statistical Analysis

Values are given as the mean ± s.d. Data were expressed in terms of sensitivity and specificity as well as diagnostic accuracy, with the results of quantitative coronary angiography serving as the gold standard. To evaluate receiver operating characteristics (ROC) of computer quantification, sensitivity (true-positives/number of patients with confirmed disease), specificity (true-negatives/number of patients without disease) and accuracy ((true-positives + true-negatives)/total patients) were determined for threshold settings of disease extent of 1.0, 1.5, 2.0, 2.5 and 3.0 s.d. below the normal mean and ≥50%, ≥75% and ≥90% luminal stenosis diameter. From these data, ROC curves were plotted for multiple sensitivity/specificity pairs according to the method of Metz (*18*). Curves were generated for localization to each individual vascular territory, for the non-LAD territory (e.g., LCx and RCA) and for overall disease detection.

A Student's t-test with Bonferroni's correction was used to compare continuous variables in the groups and noncontinuous variables were compared using Fisher's exact test or a chi-square test, depending on sample sizes. Statistical significance was defined as p values ≤0.05.

RESULTS

Patient Characteristics

The characteristics of the study and reference groups are summarized in Table 1. The reference group used for the normal database included five females and 13 males with a mean age of 36.7 ± 15.3 yr (median: 34 yr, range 21–77 yr).

TABLE 1
Clinical Characteristics of the Study Participants

	Study group (n = 34)	Reference group (n = 18)
Female	10 (29.4%)	5 (27.8%)*
Male	24 (70.6%)	13 (72.2%)*
Age (yr)		
Mean ± s.d.	60.6 ± 11.2	36.7 ± 15.3†
Range	38 (40–78)	56 (21–77)
Median	60.5	34
s/p MI	3	—
s/p PTCA	8	—
s/p CABG	1	—

*$p < 0.01$ versus study group.
†Nonsignificant.
MI = myocardial infarction; s/p = status post.

The study group was comprised of 24 men and 10 women with a mean age of 60.6 ± 11.2 yr (median: 60.5 yr, range 40–78 yr). There were three patients with prior myocardial infarction, eight patients with a history of PTCA and one with previous CABG. In all cases, revascularization was performed at least 6 mo prior to the study. Two male and three female healthy volunteers, based on <5% likelihood for CAD were included in this group. The difference between the mean age of the study group and the normal group was statistically significant ($p < 0.01$). There was no statistically significant difference between the sex distribution of both groups.

Angiographic Findings

Coronary angiography results for extent and localization of CAD are summarized in Table 2. Based on a threshold of ≥50% diameter stenosis, we identified 16 patients with significant narrowing of at least one coronary vessel (≥75%: 13; ≥90%: 12). Of these 16 patients, 9 had one-vessel disease, 5 had two-vessel disease and in two patients all vessels were involved (≥75%: 9, 3, 1; ≥90%: 10, 2, 0). We identified nine lesions with a mean stenosis diameter of 89.6% in the LAD territory, nine in the RCA (78.3%) and seven lesions (87.1%) in the territory of the LCx. The differences in mean stenosis diameter were not statistically significant.

Hemodynamic Findings

Of the 34 persons in the study group, 12 had dipyridamole stress testing and 22 others received adenosine. All subjects in the reference group received adenosine. The systolic blood pressure and heart rate at rest averaged 110 ± 10 mmHg and 58 ± 8 bpm in the study group and was 115 ± 13 mmHg and 55 ± 7 bpm in the reference group. Systolic blood pressure fell by 14 ± 12 mmHg during adenosine and by 13 ± 12 mmHg during dipyridamole infusion in the study group. The changes in the reference group after adenosine infusion were 15 ± 13 mmHg and +17 ± 12 mmHg. The change of systolic blood pressure and heart rate during pharmacologic stress was significant

TABLE 2
Angiographic Patterns of CAD in 29 Patients

	% Stenosis			Stenosis diameter		
	≥50%	≥75%	≥90%	≥50%	≥75%	≥90%
	n	n	n			
Insignificant CAD	13	16	17			
Significant CAD	16	13	12			
One-vessel disease	9	9	10			
Two-vessel disease	5	3	2			
Three-vessel disease	2	1	0			
Left main CAD	1	1	0			
LAD lesions	9	7	5	89.6 ± 13.2	95.4 ± 7.1	99.6 ± 0.5
RCA lesions	9	6	6	78.3 ± 18.3	88.0 ± 9.1	93.3 ± 5.7
LCx lesions	7	5	3	87.1 ± 17.1	98.2 ± 4.0	98.2 ± 4.0

($p < 0.05$) within each group, whereas there was no statistically significant difference between the three subsets.

Four of 12 (30%) patients with dipyridamole and 13 of 40 patients (32.5%) with adenosine had chest pain or mild noncardiac symptoms. All others were asymptomatic. No patient had severe hypotension (systolic BP < 90 mmHg) and none required administration of aminophylline.

Scintigraphic Findings

Reference Group. We used the results of 18 subjects in the earlier described reference group to construct a normal polar map of ^{13}N-ammonia activity. The results of the stress studies for each myocardial wall segment and for each coronary vascular territory are displayed in Figure 5. In addition, the regional values for the rest-to-stress ratio are depicted. The relative tracer distribution throughout the left ventricle was homogeneous with values ranging from 66% to 85% during stress and rest. The inferior wall had the highest relative tracer concentration of the nine myocardial wall segments under rest and stress conditions. There was a significant difference of relative activity between proximal and distal wall segments. The activity in the distal lateral wall for both rest and stress studies was significantly lower than that of the distal septum and inferior distal walls. The lowest tracer concentration was recorded in the apex ($p < 0.05$ versus LAT and $p < 0.01$ versus all other segments), whereas all other possible comparisons did not reach statistical significance. There was no statistically significant difference in tracer distribution dependent on gender in patients without CAD. The ratio map shown in Figure 5 demonstrated homogeneous values ranging from 1.00 ± 0.24 to 1.06 ± 0.15. There was no significant difference between values in the lateral wall and the remaining segments of the left ventricle.

Patient Example. Figure 6 shows the scintigraphic results in a 61-yr-old man who was referred to our institution for evaluation of suspected CAD. Quantitative coronary angiography demonstrated a stenosis diameter of 99% in the LAD and a normal circumflex and RCA. Rest, stress, rest-stress, and rest-to-stress comparison maps of this patient are shown in Figure 6. The stress polar map depicts an anterior-apical defect, whereas the rest image shows only subtle defects. The ratio map (right) delineates the apical defect. Three-dimensional displays of the stress, rest and ratio of the same patient are shown in the upper panel. Figure 7 depicts the comparison of an individual patient with the normal database. All white pixels are within 2 s.d., whereas the color code represents the degree of standardizations.

Detection of CAD. The results for detection of CAD using varying standard deviation criteria are summarized in Table 3. By a threshold of ≥75% stenosis diameter within a given vascular territory, the highest diagnostic accuracy (85%) for detection of CAD was observed for a cutoff of 2.0 s.d.s for computing the ratio map (rest-to-stress). Sensitivity was 93% and specificity 80%. By using the difference map (rest-stress), the highest diagnostic accuracy was also observed with 2.0 s.d.s, thus yielding a sensitivity of 86% and a specificity of 80%. Use of the stress information alone resulted in a diagnostic accuracy of 82% with a sensitivity of 79% and a specificity of 85%. Table 4 summarizes the diagnostic performance using 50%, 75% and 90% stenosis diameter thresholds and a 2.0 s.d. cutoff.

Localization of Disease. ROC curves for localization of coronary artery stenosis for stress, rest, rest-stress, and rest-to-stress are shown in Figure 8 for each individual vascular territory (angiographic threshold: ≥75% narrowing). The highest diagnostic accuracy for localization of

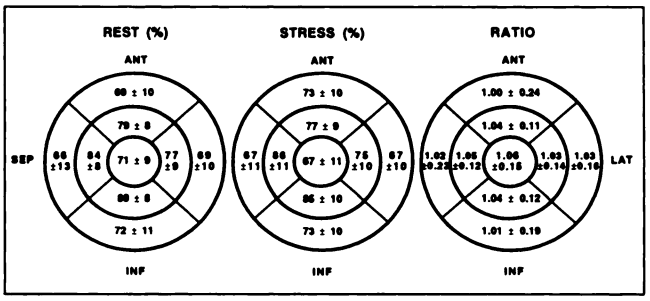

FIGURE 5. Relative tracer distribution under stress and rest conditions in the reference group, used as "normal polar map", segmented according to proximal and distal myocardial wall segments. Relative activity is expressed in percent ± s.d. The right map depicts regional ratio values of rest and stress activity. ANT = anterior; SEP = septal; INF = inferior; LAT = lateral.

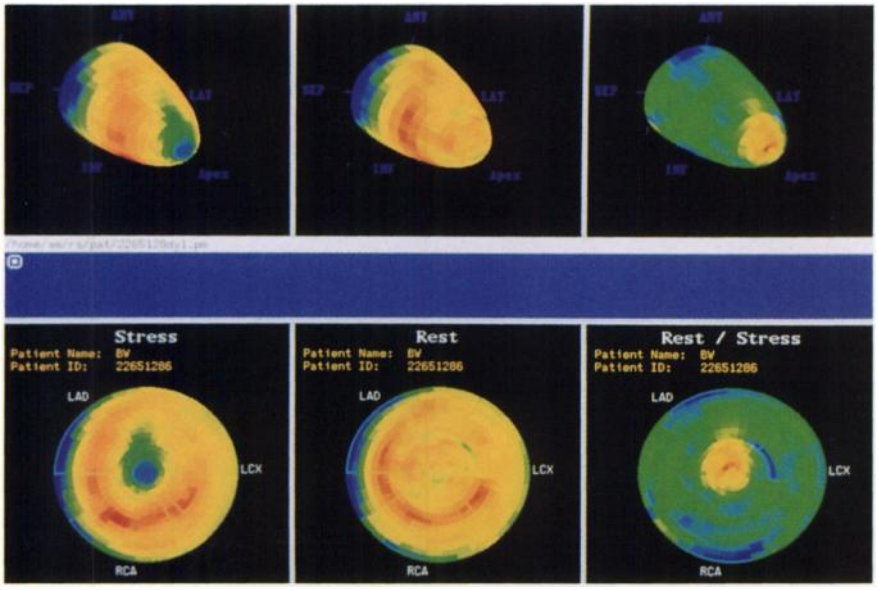

FIGURE 6. Stress and rest polar maps and ratio polar maps (lower panel) of a 61-yr-old male with 99% narrowing of the LAD. The stress-induced apical defect is clearly demonstrated. The upper panel displays three-dimensional representation of the same data.

CAD in the LAD territory (91%) was found using the stress polar map and 2.0 s.d.s, which yielded a sensitivity of 86% and a specificity of 93%. Calculation of difference or ratio maps at this standard deviation reached an accuracy of 82% and 85%, respectively. The best results for the LCx territory were observed using the ratio map and 2.0 s.d.s, which yielded an accuracy of 79%, a sensitivity of 80% and a specificity of 79%. The diagnostic accuracy was 79% for stress and rest maps and 76% for the difference polar map. In the RCA territory, stress and difference polar maps produced identical results for 2.0 s.d.s (accuracy 88%, sensitivity 83%, specificity 89%). The corresponding results for angiographic thresholds of ≥50% and ≥90% are given in Table 4.

Interobserver and Intraobserver Variability. Two observers analyzed all PET studies without prior knowledge of the patients' histories or coronary angiography results. One observer analyzed the data twice after a waiting period of 2 wk. As shown in Figure 9, there was a very high correlation (r = 0.97–0.99) between the results of the first and second analysis of observer 2, which yielded a very low intraobserver variability for all three vascular territories. The correlation between observers 1 and 2 was in the same range for the LAD (r = 0.98) and LCx territory (r = 0.97). The lowest correlation coefficient for interobserver comparison was found in the RCA territory (r = 0.82). By using a threshold of ≥10% abnormal pixels within each vascular territory below 2.0 of the normal mean, both observers agreed in 29 of 34 (85.3%) patients in detection of CAD. The intraobserver agreement was 97.1% (Table 5). For further evaluation, we calculated the intraobserver and interobserver agreement for each individual vascular territory (Table 5) and found consistent values for the LAD and LCx territory (94.1%–97.1%). The intraobserver agreement for localization of disease in the RCA region was 94.1%. The largest disagreement between both observers

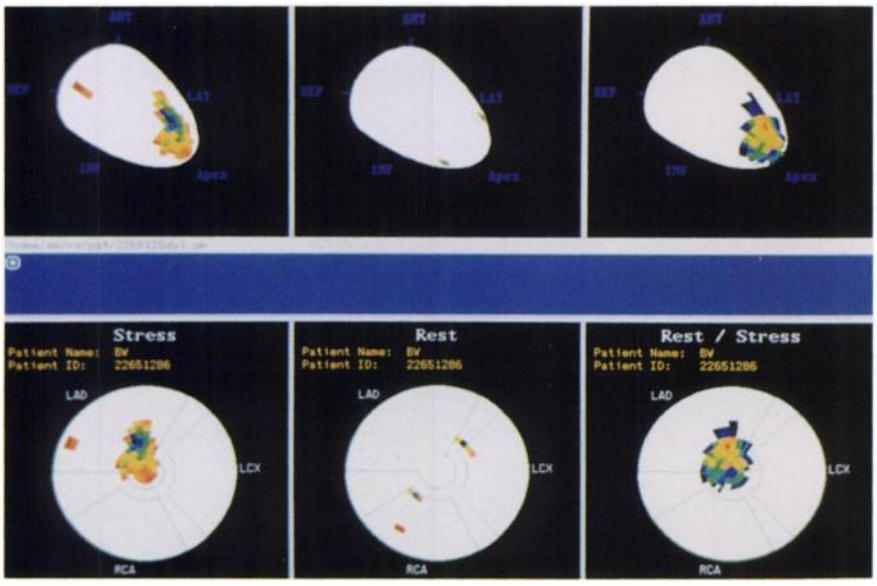

FIGURE 7. Data of the same patient shown in Figure 6 compared to the normal database using polar map (below) or three-dimensional display (above). The white area represents values within 2 s.d. of the normal population, whereas the color code represents the severity of the perfusion abnormality in standard deviations.

TABLE 3

Sensitivity, Specifity and Accuracy for Stress-, Rest-, Rest-Stress- and Rest-to-Stress-Evaluation for CAD Detection and Vascular Territory Recognition as a Function of Standard Deviations Below the Mean of a Normal Database (Thresholds: Abnormal Region ≥ 10% of Vascular Territory; Stenosis Diameter ≥ 75%)

	Stress					Rest					Rest-Stress				Rest-to-Stress			
s.d.	1.0	1.5	2.0	2.5	3.0	1.0	1.5	2.0	2.5	3.0	1.0	1.5	2.0	2.5	1.0	1.5	2.0	2.5
LAD																		
sens	1.00	0.86	0.86	0.86	0.29	0.43	0.29	0.00	0.00	0.00	1.00	0.86	0.71	0.57	1.00	1.00	0.86	0.86
spec	0.63	0.78	0.93	0.93	1.00	0.63	0.81	0.93	1.00	1.00	0.41	0.78	0.85	0.89	0.48	0.74	0.85	0.85
acc	0.71	0.79	0.91	0.91	0.85	0.59	0.71	0.74	0.79	0.79	0.53	0.79	0.82	0.82	0.59	0.79	0.85	0.85
LCx																		
sens	0.80	0.60	0.60	0.40	0.40	0.40	0.20	0.20	0.20	0.20	0.80	0.80	0.80	0.60	0.80	0.80	0.80	0.60
spec	0.59	0.76	0.83	0.83	0.86	0.72	0.83	0.90	0.93	1.00	0.34	0.52	0.76	0.86	0.38	0.62	0.79	0.79
acc	0.62	0.74	0.79	0.79	0.79	0.68	0.74	0.79	0.82	0.88	0.41	0.56	0.76	0.82	0.44	0.65	0.79	0.76
RCA																		
sens	0.83	0.83	0.83	0.83	0.67	0.83	0.83	0.83	0.83	0.50	1.00	0.83	0.83	0.67	1.00	1.00	0.83	0.67
spec	0.25	0.43	0.89	0.93	0.96	0.32	0.54	0.79	0.86	0.93	0.39	0.71	0.89	0.93	0.36	0.64	0.82	0.93
acc	0.35	0.50	0.88	0.91	0.91	0.41	0.59	0.79	0.85	0.85	0.50	0.74	0.88	0.88	0.47	0.71	0.82	0.88
Det																		
sens	1.00	0.93	0.79	0.79	0.50	0.86	0.64	0.43	0.43	0.21	1.00	0.93	0.86	0.64	1.00	0.93	0.93	0.79
spec	0.25	0.45	0.85	0.85	0.85	0.30	0.40	0.65	0.75	0.90	0.25	0.50	0.80	0.85	0.25	0.50	0.80	0.75
acc	0.56	0.65	0.82	0.82	0.71	0.50	0.53	0.56	0.62	0.62	0.56	0.68	0.82	0.76	0.56	0.68	0.85	0.76

sens = sensitivity; spec = specificity; acc = accuracy; Det = detection of CAD.

was found in the inferior wall with an agreement rate of 79.4%.

DISCUSSION

Several quantitative approaches for the interpretation of cardiac SPECT imaging have been introduced and are widely used for the evaluation of cardiac perfusion studies (*1,4,5,19,20*). Objective criteria for perfusion abnormalities and low interobserver variability make such approaches a useful tool in the diagnostic work-up of patients with suspected or proven CAD. Quantitative methods for the analysis of scintigraphic data lend themselves even better to data derived by PET. High spatial resolution and attenuation correction limits inhomogeneities in tracer distribution due to partial volume effect and tissue attenuation often observed with ^{201}Tl SPECT imaging (*5,6,21*). Therefore, we hypothesized that quantification of regional tracer activity should yield high diagnostic specificity for CAD detection by PET because the incidence of imaging artifacts is greatly reduced.

TABLE 4

Sensitivity, Specificity and Accuracy for Stress-, Rest-, Rest-Stress- and Rest-to-Stress-Evaluation for CAD Detection and Vascular Territory Recognition as a Function of Quantitatively Determined Stenosis Diameter (Thresholds: 10% Extent of the ROI, ≥2.0 s.d.s)

	Stress			Rest			Rest-Stress			Rest-to-Stress		
	≥50%	≥75%	≥90%	≥50%	≥75%	≥90%	≥50%	≥75%	≥90%	≥50%	≥75%	≥90%
LAD												
sens	0.78	0.86	0.80	0.11	0.00	0.00	0.67	0.71	0.60	0.78	0.86	0.80
spec	0.96	0.93	0.86	0.96	0.93	0.93	0.88	0.85	0.79	0.88	0.85	0.79
acc	0.91	0.91	0.85	0.74	0.75	0.79	0.82	0.82	0.76	0.85	0.85	0.79
LCx												
sens	0.43	0.60	0.67	0.14	0.20	0.33	0.57	0.80	1.00	0.57	0.80	1.00
spec	0.81	0.83	0.81	0.89	0.90	0.90	0.74	0.76	0.74	0.78	0.79	0.77
acc	0.74	0.79	0.79	0.74	0.79	0.85	0.71	0.76	0.76	0.74	0.79	0.79
RCA												
sens	0.67	0.83	0.83	0.67	0.83	0.83	0.67	0.83	0.83	0.67	0.83	0.83
spec	0.92	0.89	0.89	0.80	0.79	0.79	0.92	0.89	0.89	0.84	0.82	0.82
acc	0.85	0.88	0.88	0.76	0.79	0.79	0.85	0.88	0.88	0.79	0.82	0.82
Det												
sens	0.69	0.79	0.77	0.44	0.43	0.38	0.81	0.86	0.85	0.88	0.93	0.92
spec	0.83	0.85	0.81	0.67	0.65	0.62	0.83	0.80	0.76	0.83	0.80	0.76
acc	0.76	0.82	0.79	0.56	0.56	0.53	0.82	0.82	0.79	0.85	0.85	0.82

sens = sensitivity; spec = specificity; acc = accuracy; det = detection of CAD.

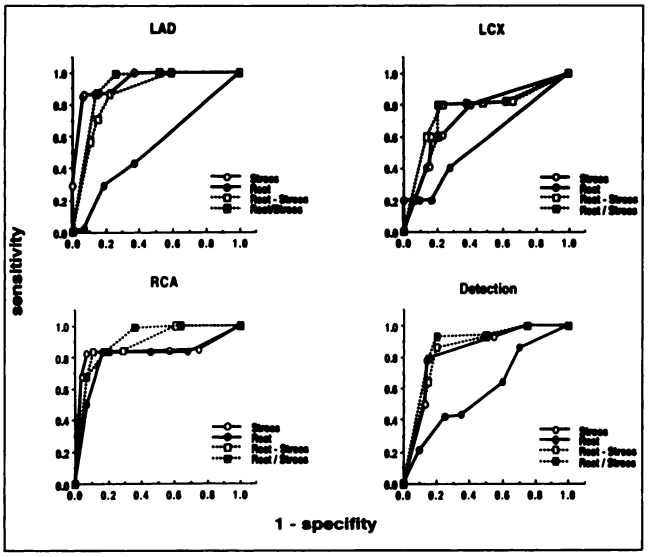

FIGURE 8. ROC curves for overall detection and localization of CAD in individual vascular territories (threshold: ≥75% stenosis diameter; ≥10% extent of ROI) by means of stress, rest, rest-stress, and rest-to-stress studies. The five data points represent varying standard deviation cutoff criteria from 3.0 to 1.0 by 0.5 increments.

Analysis software for SPECT cardiac perfusion studies commonly employs circumferential profile techniques applied to left ventricular short-axis or long-axis image planes (*13–16,22,23*). These programs are based on a two-dimensional radial search for myocardial activity originating from the center of the left ventricular cavity, which is constrained by manually defined ROIs around the heart. We have refined this technique and developed a truly three-dimensional data analysis. In taking advantage of more powerful workstations, this software does not require the generation of short-axis or long-axis image planes but relies on image volume rather than individual image planes. In addition, we introduced mathematical constraints in the search for myocardial activity to avoid the need for interactive definition of myocardial edges. In this program, the user has only to define the left ventricular long-axis and the approximate image volume in which the heart is represented. Myocardial activity is defined by a multipass search routine. Such an approach allows definition of the location of regional myocardial activity based on the anticipated shape of the left ventricle even in the presence of severe perfusion abnormalities. In addition, this searching routine permits separation of myocardial activity from adjacent liver tissue, which avidly retains ^{13}N activity. Thus, the major advantage of this software development, when compared to conventional SPECT approaches, is the automated three-dimensional delineation of myocardial activity without the need to generate short-axis and long-axis images or to define interactively the outer edge of myocardium.

Technical Considerations

The results obtained in normal volunteers and patients without angiographically proven CAD reflect the improved imaging technology provided by PET. Although it is well known that there is some regional spatial and temporal heterogeneity in myocardial blood flow even in the normal heart, this variability is generally small, being in the order of 10%–15% (*24–26*) and its detection in vivo has been limited by the spatial and temporal resolution of routinely available imaging modalities. Accordingly, we have observed a relatively homogeneous distribution of ^{13}N-ammonia activity in the myocardium as reported by others (*1–4,19,27*). There was no significant difference between a male and female population in regional tracer uptake. The implementation of attenuation correction excluded any artifacts in regional tracer distribution caused by varying body build. This is in contrast to the considerable regional variation observed with SPECT, which has been reported between the anterior and inferior walls of the left ventricle (*13–15*). The regional activity was normalized to one maximal activity value within the left ventricle. This normalization approach explains the significant differences of regional activity in the base and apex of the left ventricle. Since PET data acquisition was not ECG gated, undersampling occurred at the level of the base and apex of the left ventricle. During systole, the apical structures and basal

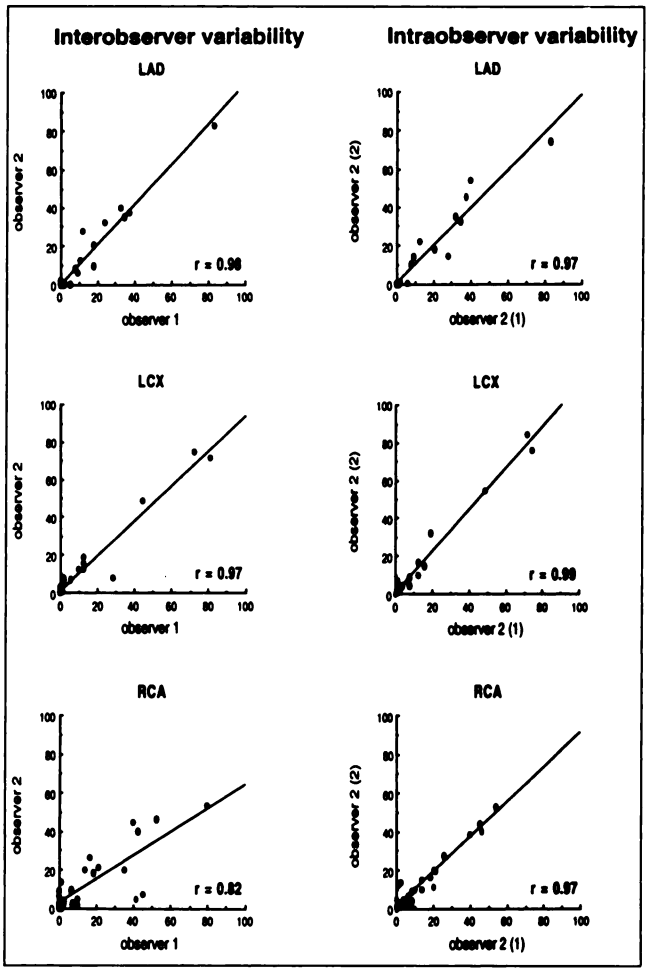

FIGURE 9. Linear regression for intraobserver and interobserver variability for localization of CAD in individual vascular territories.

TABLE 5
Intraobserver and Interobserver Agreement on Detection of CAD

		Interobserver	Intraobserver
Agreement	Disease	15	17
	No disease	14	16
		29 (85.3%)	33 (97.1%)
No agreement		5 (14.7%)	1 (2.9%)

Intraobserver and Interobserver Agreement on Localization of CAD

		LAD		LCx		RCA	
		Interobserver	Intraobserver	Interobserver	Intraobserver	Interobserver	Intraobserver
Agreement	Disease	8	8	7	6	9	12
	No disease	25	24	26	27	18	20
		33 (97.1%)	32 (94.1%)	33 (97.1%)	33 (97.1%)	27 (79.4%)	32 (94.1%)
No agreement		1 (2.9%)	2 (5.9%)	1 (2.9%)	1 (2.9%)	7 (20.6%)	2 (5.9%)

structures are moving out of the corresponding image plane and are only imaged during diastole.

Besides these anticipated variations due to nongated data acquisition, there were slight cross-sectional inhomogeneities noted by statistical analysis. The distal inferior wall displayed somewhat higher activity when compared to the septum and anterior wall, which most likely reflects the scatter of activity from neighboring organs. In contrast to ^{201}Tl or ^{82}Rb, ^{13}N-ammonia is avidly retained in hepatic tissue (*28*). In some patients, the hepatic structures are in close proximity to the heart, especially in the supine position. However, the average relative activity in the inferior wall was only 10% higher than that in the corresponding anterior wall and, again, was not changed from rest to stress studies as evidenced by the ratio map (Fig. 5).

The distal lateral wall displayed lower values of relative tracer retention than those observed in the corresponding anterior, septal and inferior segments. It has been previously observed that ^{13}N-ammonia activity in the posterolateral wall may be reduced even in the absence of any significant CAD (*29,30*). This distribution pattern is different from that of any other blood flow tracer used in combination with PET. This regional decrease of ^{13}N activity is most pronounced in transaxial image planes as recently reported by Beanlands et al. from our institution (*31*). The reasons for this regional heterogeneity of myocardial ^{13}N-ammonia distribution are unknown at the present time. It is unlikely that technical factors can be made responsible for this observation because it has not been described with ^{82}Rb or ^{15}O-water. Since ^{13}N-ammonia is retained in myocardial tissue in the form of glutamine, the most likely explanation for this inhomogeneity is the regional variation of glutamine synthetase activity. Previous studies have also shown that the distribution of ^{18}F-deoxyglucose varies regionally within the left ventricle, which suggests metabolic heterogeneity in the normal human heart (*32,33*).

Detection of CAD

The application of this analysis approach in patients with proven CAD provided first insights about the diagnostic performance and the optimization of criteria for differentiation of normal and diseased vascular territories. For the localization of disease, we employed an already established definition of vascular territories for the LAD, circumflex and right coronary arteries (*16*). These average vascular territories represent the typical distribution of vascular territories but do not account for individual variations in coronary anatomy. However, previous studies with SPECT have indicated that such techniques allow a relatively specific definition of disease in given vascular territories (*16,23*). This is especially true for disease in the LAD artery, whereas there is anticipated variation in the distribution of the circumflex or RCA territories.

The selected patient population represented a relatively small sample, but most patients had discretely defined coronary lesions. In addition, the incidence of previous myocardial infarction was low. Three patients had a history of myocardial infarction. The left ventricular ejection fraction of these patients was within the normal range in two, whereas one patient had a left ventricular ejection fraction of 39%. The highest diagnostic accuracy for detection of CAD was achieved using the ratio criteria comparing rest and stress tracer distribution. The sensitivity for detection of disease was 93% using this approach with a specificity of 80%. These data compare very favorably with the reported data for visual image analysis (*5,6,20,27*). These results indicate that methods which describe changes of regional activity from rest to stress may be more sensitive than absolute thresholds of regional relative tracer distribution in patients without previous myocardial infarction. This finding may be explained by the fact that the comparison of two maps in the same patient enhances stress-induced changes in relative tracer distribution and cancels potential inhomogeneity of activity caused by the imaging procedure.

Localization of CAD

Quantitative data analysis should result in consistent localization of disease as well as in more specific definition of defect extents in a given vascular territory when compared to visual analysis. As observed in the detection of CAD, the highest diagnostic value for localization of CAD

was observed using a threshold of 2 s.d. Within the three vascular territories, diagnostic accuracy was highest in the LAD and RCA, 91% and 88%, respectively. In contrast, the diagnostic accuracy for the circumflex artery territory was 79% (sensitivity 60%, specificity 83%). This preliminary finding of reduced sensitivity in this territory may indicate the greater variability of tracer retention in the lateral wall of the left ventricle, but may also be caused by the relatively small number of patients with circumflex disease. There was no significant difference in the severity of coronary lesions in the three vascular territories of the patient studied.

Interobserver and Intraobserver Variability

The determination of the interobserver and intraobserver variability indicated excellent agreement between observers with regard to the extent of perfusion abnormalities as demonstrated by the high correlation coefficients comparing intraobserver and interobserver results. The agreement for disease localization was highest in the LAD and LCx territories (Table 5). However, there was low interobserver variability in the localization of RCA disease. Interobserver agreement was only 79% in the presence of a significant abnormality. The reason for this relatively high disagreement most likely reflects the difficulty in defining the inferior base of the left ventricle (Fig. 3). This definition includes, to a varying degree, the mitral valve plane and/or the membranous part of the inferior septum. The atrioventricular valve plane does not adhere to a straight line, but rather generates a complicated geometry. Therefore, a higher interobserver variability with regard to perfusion abnormalities in the inferior basal part of the left ventricle is anticipated.

CONCLUSION

Our program for the analysis of cardiac ^{13}N-ammonia PET studies represents an extension of technology applied successfully in SPECT. True volumetric data sampling, automated definition of myocardial activity and three-dimensional display of the data provide a user-friendly program with improved three-dimensional representation of the scintigraphic results. Initial validation of this approach in subjects with a low likelihood of CAD and patients with angiographically proven coronary lesions suggests the high diagnostic accuracy of this technique. Homogeneous tracer distribution in the normal population reflects PET's ability to provide attenuation correction and its promise of high diagnostic specificity. The use of multiple criteria, including the ratio of rest and stress tracer distribution, may provide not only improved detection of disease but also more accurate quantification of the extent and severity of stress-induced tracer abnormalities. Further validation of this approach in a prospective multicenter study is required prior to widespread clinical use.

ACKNOWLEDGMENTS

The authors appreciate the excellent technical support from Leslie I. Botti, CNMT, Andrew R. Weeden, CNMT, Christine J. Allman, CNMT and Edward McKenna, CNMT in performing the PET studies and the cyclotron and radiochemistry staff for preparing ^{13}N-ammonia. We thank Kate Stafford, CNMT, for the database search and Roger Blevins, PharmD of Medco Research for providing the adenosine used in this study. We also thank John Hoffman and Larry Byars of CTI PET Systems, Inc. for their technical and moral support. Finally, we thank Janis Beard for preparing the manuscript.

This work was performed during the tenure of an established investigatorship of the American Heart Association, Dallas, TX (MS) and was also supported in part by the National Institutes of Health, Bethesda, MD (RO1 HL41047-02 and RO1 HL47543-01) and by a grant from CTI, Knoxville, TN.

Dr. Laubenbacher's tenure as a research fellow at the University of Michigan was supported by the Nuklearmedizinische Klinik und Poliklinik der Technischen Universitat Muenchen, Klinikum rechts der Isar, Muenchen, Germany.

Dr. Beanlands was a fellow supported by a Medical Research Council of Canada Centennial Research Fellowship Award.

REFERENCES

1. Hutchins GD, Schwaiger M, Rosenspire KC, Kripokapich J, Schelbert HR, Kuhl DE. Non-invasive quantification of regional blood flow in the human heart using N-13 ammonia and dynamic PET imaging. *J Am Coll Cardiol* 1990;15:1032–1042.
2. Krivokapich J, Smith GT, Huang SC, et al. Nitrogen-13-ammonia myocardial imaging at rest and with exercise in normal volunteers. Quantification of absolute myocardial perfusion with dynamic positron emission tomography. *Circulation* 1989;80:1328–1337.
3. Schelbert H, Phelps M, Huang S, et al. N-13 ammonia as an indicator of myocardial blood flow. *Circulation* 1981;63:1259–1272.
4. Tamaki N, Yonekura Y, Senda M, et al. Myocardial positron computed tomography with ^{13}N-ammonia at rest and during exercise. *Eur J Nucl Med* 1985;11:246–251.
5. Go RT, Marwick TH, MacIntyre WJ, et al. A prospective comparison of rubidium-82 PET and thallium-201 SPECT myocardial perfusion imaging utilizing a single dipyridamole stress in the diagnosis of coronary artery disease. *J Nucl Med* 1990;31:1899–1905.
6. Stewart R, Schwaiger M, Molina E, et al. Comparison of rubidium-82 positron emission tomography and thallium-201 SPECT imaging for detection of coronary artery disease. *Am J Cardiol* 1991;67:1303–1310.
7. Tamaki N, Yonekura Y, Yamashita K, et al. Value of rest-stress myocardial positron tomography using nitrogen-13 ammonia for the preoperative prediction of reversible asynergy. *J Nucl Med* 1989;30:1302–1310.
8. Hicks K, Ganti G, Mullani N, Gould K. Automated quantitation of three-dimensional cardiac positron emission tomography for routine clinical use. *J Nucl Med* 1989;30:1787–1797.
9. Kotzerke J, Hicks RJ, Wolfe E, et al. Three-dimensional assessment of myocardial oxidative metabolism: a new approach for regional determination of PET-derived C-11-acetate kinetics. *J Nucl Med* 1990;31:1876–1893.
10. Sennef M, Geltman E, Gergmann S, Hartmann J. Noninvasive delineation of the effects of moderate aging on myocardial perfusion. *J Nucl Med* 1991;32:2037–2042.
11. Brown B, Josephson M, Peterson R, et al. Intravenous dipyridamole combined with isometric handgrip for near maximal acute increase in coronary flow in patients with coronary artery disease. *Am J Cardiol* 1981;48:1077–1085.
12. Marwick T, Cook S, Lafont A, Underwood D, Salcedo EE. Influence of left ventricular mass on the diagnostic accuracy of myocardial perfusion imaging using positron emission tomography with dipyridamole stress. *J Nucl Med* 1991;32:2221–2226.
13. Verani MS, Mahmarian JJ, Hixson JB, Boyce TM, Staudacher RA. Diagnosis of coronary artery disease by controlled coronary vasodilation with adenosine and thallium-201 in patients unable to exercise. *Circulation* 1990; 82:80–87.
14. Iskandrian A, Heo J, Nguyen T, et al. Assessment of coronary artery disease using single-photon emission computed tomography with thallium-201 during adenosine-induced coronary hyperemia. *Am J Cardiol* 1991;67: 1190–1194.
15. Coyne E, Belvedere D, Vande Stree P, Weiland F, Evans R, Spaccavento L. Thallium-201 scintigraphy after intravenous infusion of adenosine com-

pared with exercise thallium testing in the diagnosis of coronary artery disease. *J Am Coll Cardiol* 1991;17:1289–1294.
16. Garcia EV, Van Train K, Maddahi J, et al. Quantification of rotational thallium-201 myocardial tomography. *J Nucl Med* 1985;26:17–26.
17. Lesperance J, Hudon G, White C, Laurier J, Waters D. Comparison by quantitative angiographic assessment of coronary stenoses of one view showing the severest narrowing of two orthogonal views. *Am J Cardiol* 1989;64:462–465.
18. Metz C. Basic principles of ROC analysis. *Semin Nucl Med* 1978;8:283–298.
19. Schelbert H, Wisenberg G, Phelps M, et al. Noninvasive assessment of coronary stenoses by myocardial imaging during pharmacologic coronary vasodilation. VI. Detection of coronary artery disease in man with intravenous N-13 ammonia and positron computed tomography. *Am J Cardiol* 1982;49:1197–1207.
20. Demer L, Gould K, Goldstein R, et al. Assessment of coronary artery disease severity by positron emission tomography. Comparison with quantitative arteriography in 193 patients. *Circulation* 1989;79:825–835.
21. Tamaki N, Yonehura Y, Senda M, et al. Value and limitation of stress thallium-201 single photon positron emission computed tomography: comparison with nitrogen-13 ammonia positron tomography. *J Nucl Med* 1988; 29:1187–1188.
22. Van Train K, Berman D, Garcia E, et al. Quantitative analysis of stress thallium-201 myocardial scintigrams: a multicenter trial. *J Nucl Med* 1986; 78:17–25.
23. DePasquale E, Nordy A, DePuey E, et al. Quantitative rotational thallium-201 tomography for identifying and localizing coronary artery disease. *Circulation* 1988;77:316–327.
24. Bassingthwaighte JB, King RB, Roger SA. Fractal nature of regional myocardial blood flow heterogeneity. *Circ Res* 1989;65:578–590.
25. King RB, Bassingthwaighte JB. Temporal fluctuations in regional myocardial blood flows. *Pflügers Arch* 1989;413:336–342.
26. Wolpers H, Geppert V, Hoeft A, Korb H, Schraeder R, Hellige G. Estimation of myocardial blood flow heterogeneity by transorgan helium transport functions. *Pfleugers Arch* 1984;401:217–222.
27. Yonekura Y, Tamaki N, Senda M, et al. Detection of coronary artery disease with ^{13}N-ammonia and high-resolution positron-emission computed tomography. *Am Heart J* 1987;113:645–54.
28. Green MA, Klippenstein DL, Tennison JR. Copper(II) bis(thiosemicarbazone) complexes as potential tracers for evaluation of cerebral and myocardial blood flow with PET. *J Nucl Med* 1988;29:1549–57.
29. Berry J, Baker J, Pieper K, Hanson M, Hoffman J, Coleman R. The effect of metabolic milieu on cardiac PET imaging using fluorine-18-deoxyglucose and nitrogen-13 ammonia in normal volunteers. *J Nucl Med* 1991;32:1518–1525.
30. Baudhuin T, Melin J, Marwick T, et al. Regional uptake and blood flow variations with N-13 ammonia in normal subjects do not correlate with flow or metabolic measurements by other methods [Abstract]. *J Nucl Med* 1992; 33:837.
31. Beanlands R, Muzik O, Hutchins G, Wolfe EJ, Allman K, Schwaiger M. Heterogeneity of regional N-13 ammonia tracer distribution in the normal human heart: comparison of rubidium-82 and copper-62 PTSM. *J Am Coll Cardiol* 1992: in press.
32. Hicks R, Herman W, Kalff V, et al. Quantitative evaluation of regional substrate metabolism in the human heart by positron emission tomography. *J Am Coll Cardiol* 1991;18:101–111.
33. Gropler RJ, Siegal BA, Lee KJ, et al. Nonuniformity in myocardial accumulation of F-18 fluorodeoxyglucose in normal fasted humans. *J Nucl Med* 1990;31:1749–1756.

EDITORIAL

What Should We Expect from Cardiac PET?

As cardiac positron emission tomography (PET) matures into the clinical arena and the modality attains widespread use, it is essential that the process of image interpretation not be limited to those with years of PET experience. At first glance by the inexperienced observer, PET cardiac images appear a lot simpler to interpret than single-photon emission computed tomography (SPECT) studies. After all, for years we have been reminded of the advantages of cardiac PET over SPECT, i.e., higher spatial resolution, attenuation correction, hardly any imaging artifact compared to those reported for SPECT (*1*), in short, images that are truly quantitative. Thus, our expectations might be that PET perfusion images from normal patients are homogeneous and that any inhomogeneity, no matter how small, may be safely interpreted as a perfusion defect. Moreover, upon learning this simple rule, we are safe to correlate these PET perfusion studies against the "gold standard," coronary arteriography, and that we should expect the nearly perfect accuracy reported by some investigators (*2,3*).

For those making the transition from cardiac SPECT to PET, it is important to understand that much of the experience gained in SPECT is transferable to PET, but nevertheless, there is another set of rules that needs to be learned for this new modality. It is desirable that tools be developed that assist the PET neophyte in interpreting these studies and that these tools resemble those used in SPECT. Previously, Hicks et al. (*4*) reported on the use of polar maps to quantify paired cardiac PET studies to analyze size of perfusion defect, intensity, statistical significance of and changes in perfusion or metabolism, including comparison to a normal database. This methodology also included comparison of stress-stress images to evaluate progression/regression of stenosis, early and late resting rubidium images for determining myocardial viability based on ^{82}Rb washout kinetics and perfusion-metabolic comparisons for quantifying ischemia, viability and necrosis after acute myocardial infarction.

In this issue of the *Journal*, Laubenbacher et al. report on another automated polar map analysis program, this time for the evaluation of cardiac ^{13}N-ammonia perfusion PET studies (*5*). As with other similar techniques reported for SPECT (*6–8*), one of the main expectations of this approach is to increase the objectivity of the interpretation and to reduce interobserver and intraobserver variability, two attributes particularly helpful to the PET neophyte. Their approach features several technical advancements, including a three-dimensional sampling and surface display of myocardial activity similar to more recent SPECT approaches (*9,10*) but without the need to generate oblique angle images. The approach reported by Laubenbacher et al. (*5*) uses a normal

Received Mar. 5, 1993; revision accepted Mar. 5, 1993.

For correspondence or reprints contact: Ernest V. Garcia, PhD, PET Center, Emory University School of Medicine, 1364 Clifton Rd., NE, Atlanta, GA 30322.